Adaptive λτ-Space Representation of Images and Edges

BINNUR KURT, H. TAHSIN DEMIRAL
Computer Engineering Department
Istanbul Technical University
Maslak, 80626, Istanbul
TURKEY
{kurt,demiral}@cs.itu.edu.tr http://www.cs.itu.edu.tr/~{kurt,demiral}

Abstract: - In this study, we propose an adaptive scheme for the representation of images and edges in λτ-space [1] introduced by Gökmen and Jain. The space, called λτ-space, is comprised of two dimensions: the scale dimension and the continuity dimension, controlling the smoothness and the continuity of the surface, respectively. The representation is obtained simply by filtering the image with the filter denoted as R(x,y;λ,τ). It has been shown that the representation is richer than the classical scale-space representation. But the authors in [1] adopted a linear one dimensional algorithm unable to fully exploit the properties of the representation. In our proposed scheme, we allow the space parameters, λ and τ, to vary through the image respecting the feature directions. Also we apply iterative smoothing scheme in which an image is smoothed at each iteration by controlling the space parameters also in time. The first aspect of the algorithm is connected with the robustness to noise. The second aspect of the algorithm concerns the way it treats the direction of the edges. The relation between the proposed algorithm and the anisotropic diffusion is also established in this study. The proposed representation and edge detection have been tested both qualitatively and quantitatively on various real and synthetic images. Experimental results are presented including an analysis of the introduced scheme and the behavior of the edges.

Key-Words: - λτ-space, scale space, nonlinear partial differential equations, nonlinear diffusion, smoothing, image enhancement, edge detection.
CSCC'99 Proceedings: - Pages 3011-3017

1 Introduction

Our purpose in this study is to introduce the adaptive scheme for λτ-space representation using regularization and partial differential equation framework. Nonlinear partial differential equations have been attracted great interest in solving many low-level image processing and computer vision problems including image restoration [3,4], edge detection [5,6], stereo [7] and curve evaluation [8,9]. This is due to their ability of modeling the image in continuous domain and high accuracy and stability properties when discretized.

Partial differential equations mostly arise from regularization stemming from the formulation of image processing problems as energy functionals. Regularization is a general framework used to convert an ill-posed problem to well-posed by restricting the class of admissible solutions using constraints such as smoothness. Smoothness could be imposed in the form of derivatives of the solution. Gökmen and Jain presented a method ([1]) based on regularization with filters in which regularization term consists of first and second order partial derivatives of the solution. First order derivatives correspond to membrane model and second order derivatives correspond to thin plate model. The smoothing filter, $R_{\lambda\tau}(x,y)$, associated to the functional is obtained by solving Euler-Lagrange equation resulting in forth-order partial differential equation. These filters and their properties are investigated in [2]. λτ-space representation of images and edges are formed by convolving the image with the filter, $R_{\lambda\tau}(x,y)$.

One major drawback of the algorithm is that space parameters are constant throughout the image space causing the edges to be blurred while noise is removed elsewhere. This problem is due to the linear nature of the representation.

To overcome this problem, we present an adaptive λτ-space image and edge representation allowing the space parameters, λ and τ, to vary through the image respecting the feature directions.

Our approach involves two coupled PDE's modeling inhomogeneous membrane and thin-plate functionals expressed in $\eta\xi$-directions where η and ξ are the tangent direction and the normal direction

We begin this paper with a brief overview to the $\lambda\tau$-space representation. The algorithm is then developed in Section 3. Implementation details and the experimental results on synthetic and natural data are presented in Section 4. Finally, we conclude in Section 5.

2 Overview

Image representation aims at producing images with different details. This is one of the most challenging issue in computer vision and image processing due to lack of a robust representation. In general, representations can be classified as linear and nonlinear. Linear representations are constructed by convolving the image by linear filters (kernels) with varying scales. For instance, in classical scale-space the kernel is a Gaussian and the scale-space representation is constructed either by convolving the image by a Gaussian with increasing standard deviation or by solving the linear heat equation in time. This representation is causal, since the isotropic heat equation satisfies a maximum principle. However, the Gaussian scale-space suffers from serious drawbacks such as over-smoothing and location uncertainty along edges at large scales due to interactions between nearby edges and displacements. Smoothing is done in a homogeneous fashion at the same rate in all directions. This results in blurring of edges at the same rate as smoothing of object interiors. Such a filter results in poor edge localization. A representation which is known to be richer than the Gaussian scale-space is $\lambda\tau$-space representation in which the kernel is derived from the hybrid functional:

$$E(u) = \iint_{\Omega} (u-d)^2 + \lambda[(1-\tau)(u_x^2 + u_y^2) + \tau(u_{xx}^2 + 2u_{xy}^2 + u_{yy}^2)]d\Omega$$

where d(x,y) is the given image, λ is the real-valued regularization parameter and $\tau \in [0,1]$ is the real-valued continuity control parameter. Here, the hybrid functional is used to obtain a smooth transition from membrane model to the plate model. Note that, for τ=0, the functional reduces to the membrane model, for τ=1 it reduces to the plate model, and for the intermediate values of this parameter we obtain hybrid surfaces. In order to obtain these hybrid surfaces, the solution of the Euler-Lagrange equation associated the hybrid functional is needed. The derivation of these solutions and their analysis are given in [2].

The $\lambda\tau$-space representation is capable of producing larger numbers of images each of which have different characteristics of details. However the use of constant space parameters throughout the image causes the edges to be blurred for large λ values regardless of the τ dimension. Next chapter deals with this problem, introducing anisotropic $\lambda\tau$-space representation.

3 Adaptive Scheme

Recall that the hybrid functional is comprised of two terms containing first- and second-order derivatives of the solution along x and y directions. We denote these terms as

$$E_1(u) = \iint_{\Omega} \|\nabla u\|^2 d\Omega \quad (1)$$

$$E_2(u) = \iint_{\Omega} \|Hu\|^2 d\Omega \quad (2)$$

where H designates the Hessian operator. The hybrid functional is defined as a linear combination of these two terms

$$E(u) = (1-\tau)E_1(u) + \tau E_2(u)$$

Minimization of the functionals (1) and (2) separately yields the following PDE's

$$\frac{\partial u}{\partial t} = \Lambda(\lambda(\|\Lambda u\|))\,\Lambda^T(u))$$

$$\frac{\partial u}{\partial t} = \Lambda\Lambda^T(\lambda(\|\Lambda u\|)\,\Lambda\Lambda^T(u)))$$

where the operator, Λ, is given as follows

$$\Lambda = [\frac{\partial}{\partial x}, \frac{\partial}{\partial y}] \quad (6)$$

such that

$$\Lambda(g) = [\frac{\partial g}{\partial x}, \frac{\partial g}{\partial y}] \hat{=} \nabla g \ , \ (\Lambda(g))^{\mathrm{T}} = \Lambda^{\mathrm{T}}(g)$$

$$\Lambda(\begin{bmatrix} f \\ g \end{bmatrix}) = \frac{\partial f}{\partial x} + \frac{\partial f}{\partial y}$$

$$\Lambda\Lambda^{\hat{O}} \hat{=} \Delta \quad , \quad \Lambda^{\hat{O}}\Lambda \hat{=} H \ ,$$

and

$$u(x, y;0) = d(x, y)\,.$$

The quasi-linear PDE given in the equation (4) is the anisotropic (inhomogeneous) diffusion proposed by Perona and Malik [5]. λ is called the diffusion coefficient which is a function of the gradient of the solution, f(x,y;t), and is chosen to be a decreasing function of the gradient, $|\nabla f|$, in such a way that a higher rate of diffusion occurs for low values of $|\nabla f|$ and vice-versa. This encourages smoothing within a region in preference to smoothing across edges, thereby also performing image enhancement.

The minimization of the hybrid functional (3) can be easily derived from the PDE's (4) and (5) as

$$\begin{aligned}\frac{\partial u}{\partial t} = (1-\tau)\Lambda(\lambda_{\mathrm{m}}(\|\Lambda u\|)\,\Lambda^{\mathrm{T}}(u)) + \\ \tau\Lambda\Lambda^{\mathrm{T}}(\lambda_{\mathrm{p}}(\|\Lambda u\|)\,\Lambda\Lambda^{\mathrm{T}}(u))\end{aligned} \tag{8}$$

Equation (8) consists of the linear combination two diffusion processes whose fluxes are controlled by the λ_{m} and λ_{p} functions of the gradient. When the image is corrupted by noise of high variance, higher gradient terms are required to robust estimation of the local image features such as edges and corners. In order to control the direction of diffusion allowing minimal smoothing in the direction across to the image features, and maximal smoothing in the direction normal to the image features, we express the hybrid diffusion in $\eta\xi$-form such that new directional operators, Λ_η and Λ_ξ, are defined as

$$\Lambda_\eta \triangleq \eta\Lambda$$
$$\Lambda_\xi \triangleq \xi\Lambda$$

where

$$\eta = \frac{\lfloor u_x, u_y \rfloor}{\sqrt{u_x^2 + u_y^2}}, \quad \xi = \frac{\lfloor -u_y, u_x \rfloor}{\sqrt{u_x^2 + u_y^2}}$$

Also note that

$$\Lambda(u) = \Lambda_\eta(u)\varsigma + \Lambda_\xi(u)\xi$$
$$\Lambda(\Lambda^{\mathrm{T}}(u)) = \Lambda_\eta(\Lambda_\eta(u)) + \Lambda_\xi(\Lambda_\xi(u))$$

Rewriting the hybrid diffusion given in the equation (8) in terms of the directional operators yields

$$\begin{aligned}\frac{\partial u}{\partial t} = (1-\tau)\{[\lambda_{\mathrm{m}} + \|\Lambda u\|\lambda'_{\mathrm{m}}]\Lambda_\eta(\Lambda^{\mathrm{T}}{}_\eta(u)) + \\ \lambda'_{\mathrm{m}}\Lambda_\xi(\Lambda^{\mathrm{T}}{}_\xi(u))\} + \\ \tau\{\Lambda\Lambda^T(\lambda_{\mathrm{p}}(\|\Lambda u\|))\,\Lambda\Lambda^T(u) + \\ \lambda_{\mathrm{p}}(\|\Lambda u\|)\,\Lambda\Lambda^T(\Lambda\Lambda^T(u))\}\end{aligned} \tag{9}$$

or in a simpler form

$$\begin{aligned}\frac{\partial u}{\partial t} = (1-\tau)\{[\lambda_{\mathrm{m}} + \|\Lambda u\|\lambda'_{\mathrm{m}}]u_{\eta\eta} + \lambda_{\mathrm{m}}u_{\xi\xi})\} + \\ \tau\{[\lambda_{\mathrm{p}} + \|\Lambda u\|^2\Delta\lambda_{\mathrm{p}}]u_{\eta\eta\eta\eta} + \lambda_{\mathrm{p}}u_{\xi\xi\xi\xi}\}\end{aligned} \tag{10}$$

where

$$\begin{aligned}u_{\eta\eta} &= \frac{u_x^2u_{xx} + 2u_xu_yu_{xy} + u_y^2u_{yy}}{(u_x^2 + u_y^2)} \\ u_{\xi\xi} &= \frac{u_y^2u_{xx} - 2u_xu_yu_{xy} + u_x^2u_{yy}}{(u_x^2 + u_y^2)} \\ u_{\eta\eta\eta\eta} &= \frac{u_x^2u_{xxxx} + 2u_xu_yu_{xxxy} + (u_x^2 + u_y^2)u_{xxyy} + 2u_xu_yu_{xyyy} + u_y^2u_{yyyy}}{(u_x^2 + u_y^2)} \\ u_{\xi\xi\xi\xi} &= \frac{u_y^2u_{xxxx} - 2u_xu_yu_{xxxy} + (u_x^2 + u_y^2)u_{xxyy} - 2u_xu_yu_{xyyy} + u_x^2u_{yyyy}}{(u_x^2 + u_y^2)}\end{aligned} \tag{11}$$

The functions λ_{m} and λ_{p} control the amount and the direction of smoothness such that for large values of the gradient, $|\nabla f|$, we allow less diffusion and vice-versa, and in the gradient direction, η, we have always smaller amount of diffusion due to the additive term inversely proportional to the gradient. Note that for τ=0, the diffusion reduces to the Perona-Malik equation, for τ=1 it reduces to the second-order diffusion, and for intermediate values of this parameter we obtain the surfaces corresponding to the hybrid diffusion.

Next chapter deals with the discretization issues of the hybrid diffusion.

4 Implementation and Results

In this section, we briefly mention on the discretization of the partial differential equation given in (10) by using finite differences. At each instance of time, the function u(x,y;t+1) is evaluated through the forth-order procedure:

$$\frac{\partial u(x, y; t)}{\partial t} = V^{(t)}(u(x, y; t))(k) - V^{(t)}(u(x, y; t))(k-1)$$

$$\frac{\partial^2 u}{\partial x^2} = \frac{\partial}{\partial x}(V(u)(i,j) - V(u)(i-1,j))$$
$$= V(\frac{\partial u}{\partial x})(i,j) - V(\frac{\partial u}{\partial x})(i-1,j)$$

$$\frac{\partial^4 u}{\partial x^4} = \frac{\partial^2}{\partial x^2}(V(u)(i+1,j) + V(u)(i-1,j) - 2V(u)(i,j))$$
$$= V(\frac{\partial^2 u}{\partial x^2})(i+1,j) + V(\frac{\partial^2 u}{\partial x^2})(i-1,j) - 2V(\frac{\partial u}{\partial x})(i,j)$$

where T(.)(k) denotes the value of the function of *t* at k and V(.)(i,j) denotes the value of the function of (*x*,*y*) at (i,j).

The functions λ_m and λ_p are chosen as

$$\lambda_m(\|\Lambda(u)\|;t) = \frac{1}{1+\left(\frac{\|\Lambda(u)\|}{K(t)}\right)^2}$$

$$\lambda_p(\|\Lambda(u)\|;t) = \exp(-\left(\frac{\|\Lambda(u)\|}{K(t)}\right)^2)$$

where the function K(t) is a decreasing function of time. The effect of K(t) on the solution is studied in [10]. We have used a linear function, $K(t)=K_{max}-\alpha t$, in our experiments where $\alpha=(K_{max}-K_{min})/T$ and T is the diffusion time.

The algorithm was tested on 8 bit gray level images. We now present these results on synthetic and real images. In order to evaluate detection and localization performance, we used noisy checkerboard image with nmse=41.06. The original and noisy checkerboard images are shown in Figure 1. Surfaces and detected edges for three τ values (0.0, 0.5, and 1.0) are shown in Figure 2. We calculated the conditional probability of a detected edge pixel given an ideal edge pixel, *Pr*{*DE*|*IE*}, the conditional probability of an ideal edge pixel given a detected edge pixel, *Pr*{*IE*|*DE*}, the mean square distance (MSD) between ideal and detected edge pixels [11] and the Pratt's Figure Of Merit (FOM). These performance indices for checkerboard images degraded at different amounts are given in Table 1.

(a) (b)

Figure 1 (a) Original checkerboard image
(b) Noisy checkerboard image

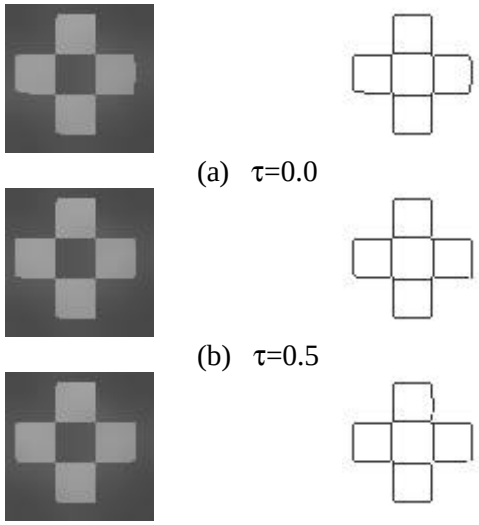

(a) τ=0.0

(b) τ=0.5

(c) τ=1.0

Figure 2 Reconstructed surfaces and detected edges for τ=0.0, 0.5, and 1.0.

Table 1 Quantitative results for noisy checkerboard Images

MSE	41.06			30.47			25.43		
τ	0	0.5	1.0	0	0.5	1.0	0	0.5	1.0
Pr{IE|DE}	0.94	0.97	0.95	0.97	0.97	0.99	0.99	0.99	0.99
Pr{IE|DE}	0.95	0.98	0.97	0.98	0.99	0.99	0.99	0.99	0.99
MSD	0.22	0.13	0.17	0.13	0.11	0.06	0.08	0.06	0.06
FOM	0.94	0.98	0.95	0.97	0.97	0.99	0.99	0.99	0.99

Table 2 Quantitative results for noisy checkerboard Images

MSE	41.06			30.47			25.43		
τ	0	0.5	1.0	0	0.5	1.0	0	0.5	1.0
MSE	14.4	13.0	13.6	8.7	9.4	7.6	5.8	4.4	4.2
NMSE	0.31	0.28	0.30	0.19	0.20	0.16	0.12	0.09	0.09

For highly noisy images the detected edges for τ=0.5 are always better in the sense of the performance indices introduced above while in other cases the results for τ=1.0 are better.

Table 2 contains mean square error (MSE) and normalized mean square error (NMSE) between the reconstructed and the original surfaces. The reconstructed surfaces obtained for τ=0.5 result in smaller MSE for highly noisy images. As compared to the Perona-Malik`s diffusion, hybrid diffusion always results in better replica of the original image.

Finally, we present a comparison of the proposed scheme and linear λτ-space representation and generalized edge detector (GED). We see that for the case of no noise (Figure 5,8), the proposed algorithm performs as well as GED and in the presence of high noise (Figure 4,7), it performs much better than GED. The original and noisy

Airfield and Bridge images are given in Figure 3 and in Figure 6, respectively.

5 Summary and Conclusions

We have presented nonlinear image and edge representation derived from the λτ-space representation in which the space parameters are adaptively determined controlling the amount and the direction of smoothness. We have showed experimentally that our proposed scheme is capable of locating the feature direction robustly when the both terms in the hybrid diffusion are used as contrary to the Perona-Malik equation. The edge detection performance has been assessed by using quantitative measures such as FOM (Figure-Of-Merit), missing and false alarm characteristics with promising results.

We have experimentally showed that introduced diffusion mechanism provides additional details when compared to the Perona-Malik's diffusion. Using this approach one may obtain edges and surfaces having different characteristics for the choice of different τ's.

Acknowledgements

We are grateful to M. Gökmen for many useful discussions regarding this work.

References:

[1] Muhittin Gökmen, Anil K. Jain, λτ-Space Representation of Images and Generalized Edge Detector, *IEEE Trans. on PAMI*, Vol. 19, No. 6, 1997, pp. 545-563.

[2] Binnur Kurt, Muhittin Gökmen, Two Dimensional Generalized Edge Detector, submitted to *Int. Conf. On Image Analysis and Processing*, ICIAP'99. (http://www.cs.itu.edu.tr/~kurt/iciap99.ps.Z)

[3] F. Torkomani-Azar and K.-E. Tait, Image Recovery Using the Anisotropic Diffusion Equation, *IEEE Trans. On Image Processing*, , Vol. 11, No. 2, 1997, pp. 1573-1577.

[4] René A. Carmona, Sifen Zhong, Adaptive Smoothing Respecting Feature Directions, *IEEE Trans. On Image Processing*, , Vol. 7, No. 3, 1998, pp. 353-358.

[5] P. Perona and J. Malik, Scale-space and Edge Detection using Anisotropic Diffusion, *IEEE Trans. on PAMI*, Vol. 12, 1990, pp. 629-639.

[6] F. Catte, P.-L. Lions, J.-M. Morel, and T. Coll, Image Selective Smoothing and Edge Detection by Nonlinear Diffusion, *SIAM J. Numerical Analysis*, Vol. 29, 1992, pp. 182-193.

[7] O. Faugeras and R. Keriven, Variational Principles, Surface Evaluation, PDE's and the Stereo Problem, *IEEE Trans. On Image Processing*, , Vol. 7, No. 3, 1998, pp. 336-344.

[8] J. Shah, A Common Framework for Curve Evaluation, Segmentation and Anisotropic Diffusion, *IEEE Proc. Conf. Computer Vision and Pattern Recognition*, San Francisco, CA, June 1996, pp. 136-142.

[9] L. Moisan, Affine Plane Curve Evolution: A Fully Consistent Scheme, *IEEE Trans. On Image Processing*, , Vol. 7, No. 3, 1998, pp. 411-420.

[10] X. Li and T. Chen, Nonlinear Diffusion with Multiple Edginess Thresholds, *Pattern Recognition*, Vol. 27, No. 8, 1994, pp. 1029-1037.

[11] M. Gökmen and C. Li, Multiscale Edge Detection using first-order R-filter, *Proc.Int. Conf. on Pattern Recognition*, 1992, pp. 307-310.

(a)

(b)

Figure 3
(a) Original Airfield image
(b) Degraded Airfield image with Gaussian noise with σ^2=451.36.

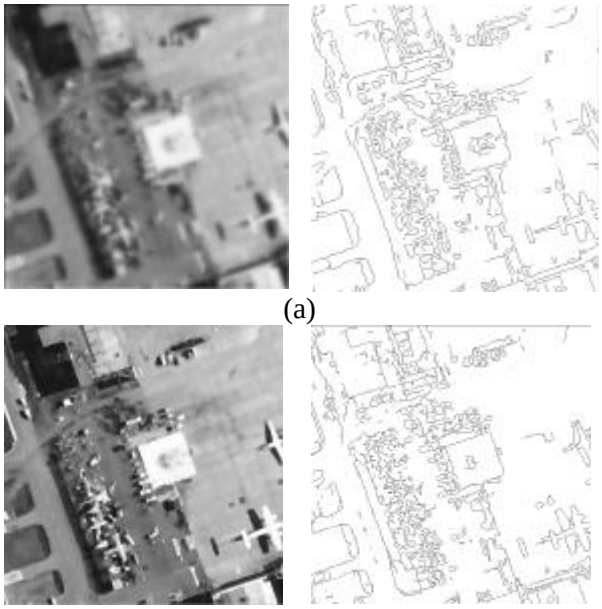

(a)

(b)

Figure 4
(a) Reconstructed surface and detected edges through the linear $\lambda\tau$-space representation.
(b) Reconstructed surface and detected edges through the proposed adaptive representation.

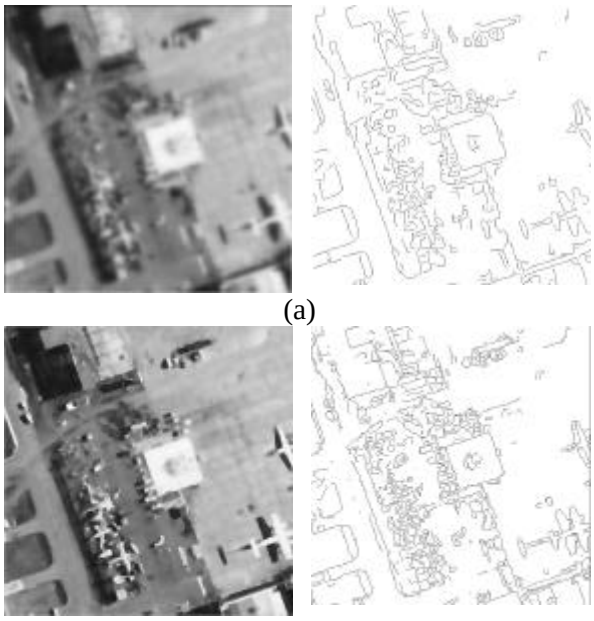

(a)

(b)

Figure 5
(a) Reconstructed surface and detected edges through the linear $\lambda\tau$-space representation.
(b) Reconstructed surface and detected edges through the proposed adaptive representation.

(a)

(b)

Figure 6
(a) Original Bridge image
(b) Degraded Bridge image with Gaussian noise with σ^2=375.73.

(a)

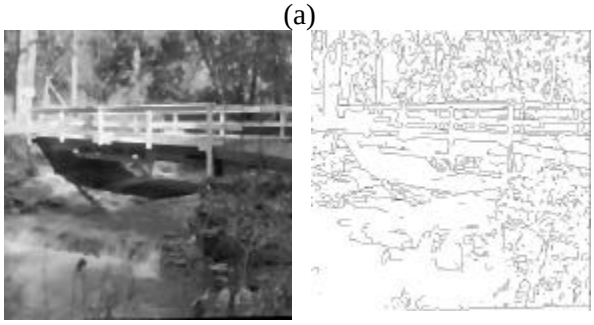

(b)

Figure 7
(a) Reconstructed surface and detected edges through the linear $\lambda\tau$-space representation.
(b) Reconstructed surface and detected edges through the proposed adaptive representation.

(a)

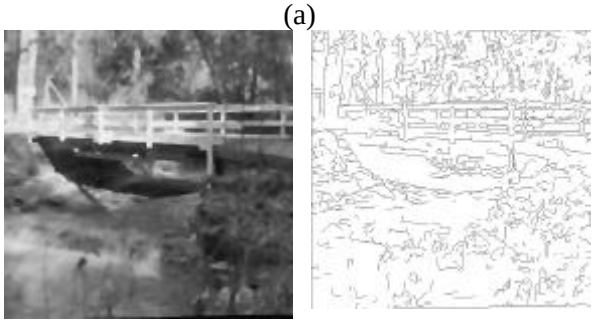

(b)

Figure 8
(a) Reconstructed surface and detected edges through the linear $\lambda\tau$-space representation.
(b) Reconstructed surface and detected edges through the proposed adaptive representation.